JOURNAL OF QUATERNARY SCIENCE (2022) **37**(4) 677–687 ISSN 0267-8179. DOI: 10.1002/jqs.3399

JQS Journal of Quaternary Science QRA Quaternary Research Association

LGM ice extent and deglaciation history in the Gurktal and Lavantal Alps (eastern European Alps): first constraints from ^{10}Be surface exposure dating of glacially polished quartz veins

ANDREAS WÖLFLER,[1]* ANDREA HAMPEL,[1] ARMIN DIELFORDER,[1] RALF HETZEL[2] and CHRISTOPH GLOTZBACH[3]
[1]Institut für Geologie, Leibniz Universität Hannover, Hannover, Germany
[2]Institut für Geologie und Paläontologie, Westfälische Wilhelms-Universität Münster, Münster, Germany
[3]Fachbereich Geowissenschaften, Universität Tübingen, Tübingen, Germany

Received 8 September 2021; Revised 27 October 2021; Accepted 8 November 2021

ABSTRACT: Compared with the western European Alps, the ice extent during the Last Glacial Maximum (LGM) and the subsequent deglaciation history of the eastern Alps east of the Tauern Window remain less well constrained. Also, considerable discrepancies exist between the mapped LGM ice margin and the ice extent predicted by ice-sheet models. Here we present the first ^{10}Be surface exposures ages from two regions east of the Tauern Window (the Gurktal and Lavantal Alps), which provide constraints on the LGM ice extent and the deglaciation history. Our results show that the deglaciation of the Gurktal Alps occurred between 16 and 14 ka, which agrees with the predictions from ice-sheet models. In contrast, the ^{10}Be ages from the Lavantal Alps located farther east are either LGM in age or predate the LGM, indicating that these regions were ice free or only partially covered by LGM ice. This finding suggests that ice-sheet models may have overestimated the LGM ice extent in the easternmost Alps. In conclusion, our study highlights the need for more age data from the eastern Alps to refine the location of the LGM ice margin and the deglaciation history, which is also crucial for climate-evolution and postglacial-rebound models.

Introduction

During the Last Glacial Maximum (LGM), which lasted from *ca.* 26 to 20 ka (e.g. Clark *et al.*, 2009), mountainous regions worldwide including the European Alps were covered by ice domes and valley glaciers (Ehlers *et al.*, 2011). Reconstructing the former LGM ice extent and the post-LGM glacial history in these regions is crucial for a number of geoscientific research disciplines, including studies about past climate evolution, glacial impact on landscape evolution, and postglacial isostatic rebound (e.g. Kuhlemann *et al.*, 2008; Batchelor *et al.*, 2019; Sternai *et al.*, 2020). In this context, quantitative age data play an important role in relating mapped geomorphological features and sediment records to individual cold or warm periods.

In the European Alps, age constraints on the LGM ice extent and the Lateglacial history were obtained by optically stimulated luminescence (OSL) dating of proglacial sediments, radiocarbon dating of organic matter from bogs or lake sediments and surface exposure dating of moraine boulders or glacially polished bedrock and quartz veins using cosmogenic nuclides (e.g. Ivy-Ochs *et al.*, 1996, 2004, 2006a; Kelly *et al.*, 2004, 2006; Federici *et al.*, 2008 Preusser *et al.*, 2007; Darnault *et al.*, 2012; Reuther *et al.*, 2011; Starnberger *et al.*, 2011; Dielforder and Hetzel, 2014; Braumann *et al.*, 2020). Most of these data come from the western Alps (west of ~10°E) and the western part of the eastern Alps (east of ~10°E) (Fig. 1) (e.g. Ivy-Ochs *et al.*, 2006a, 2008; Kerschner *et al.*, 2006; Reuther *et al.*, 2011; Moran *et al.*, 2016a,b, 2017; Wirsig *et al.*, 2016a; Braumann *et al.*, 2020). Farther east, age data are only available at a few sites in former glacier tongue areas (Draxler, 1977; van Husen 1997; Borten-schlager, 1984; Schmidt *et al.*, 2002, 2012; Starnberger *et al.*, 2011). ^{10}Be exposure ages have only been obtained from two sites in the Tauern Window (Bichler *et al.*, 2016; Wirsig *et al.*, 2016b). As a consequence, the glacial history in this part of the European Alps remains less well resolved compared with other regions located farther west.

Regarding the LGM ice extent in the easternmost Alps, mapping studies and ice-sheet models arrived at different results. Reconstructions based on mapping of glacial geomorphological features and interpretation of sedimentary sequences indicate that the eastern LGM ice margin was located between about 14 and 14.5°E (Fig. 1, white line from Ehlers *et al.*, 2011) (van Husen, 1997, 2004, 2011). However, the glacial features and sedimentary sequences interpreted as a record of the LGM ice extent are mostly undated, i.e. age information was mostly obtained by tentative correlations with sites from other regions of the Alps where age constraints are available (Draxler, 1977, 1987; van Husen, 1977; Borten-schlager, 1984; Ivy-Ochs *et al.*, 1996, 2006a). In contrast to the mapped ice extent, the ice-sheet model of Seguinot *et al.* (2018) predicts a position of the LGM ice margin *ca.* 60–80 km farther to the east at around 15.5°E (Fig. 1, blue line). As Seguinot *et al.* (2018) noted, the greater ice extent in their model might result from an overestimation of precipitation in the easternmost Alps. However, without quantitative age constraints on the deglaciation history of the easternmost Alps, the discrepancy between mapped and modelled LGM ice extents is difficult to resolve.

Here we present ^{10}Be surface exposure ages from glacially polished quartz veins and an analysis of high-resolution digital elevation models (DEMs), which together provide constraints

*Correspondence: A. Wölfler, as above.
E-mail: woelfler@geowi.uni-hannover.de

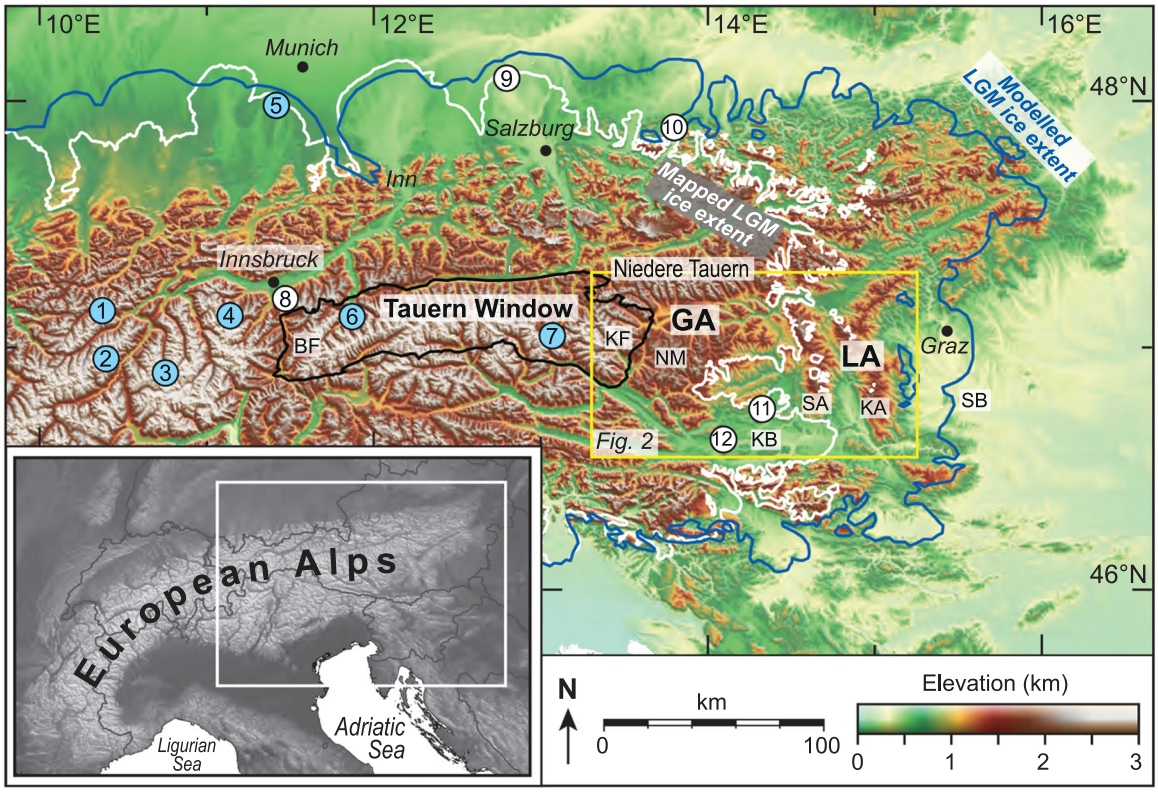

Figure 1. Topographic map of the eastern Alps (location marked by white rectangle in inset map of the European Alps). Yellow rectangle outlines the study area shown in Fig. 2 (GA: Gurktal Alps; LA: Lavantal Alps) east of the Tauern Window (marked by black line). White line indicates LGM ice margin (Ehlers *et al.*, 2011, and articles therein). Blue line shows the modelled LGM extent according to Seguinot *et al.* (2018). BF: Brenner normal fault; KF: Katschberg normal fault; NM: Nock Mountains; SA: Saualpe; KA: Koralpe; KB: Klagenfurt Basin; SB: Styrian Basin. The numbers in blue circles refer to ^{10}Be chronologies in the eastern Alps; 1: Ivy-Ochs *et al.* (2006b); 2: Kerschner *et al.* (2006), Moran *et al.* (2016b), Braumann *et al.* (2020); 3: Moran *et al.* (2016a); 4: Moran *et al.* (2017); 5: Reuther *et al.* (2011); 6: Wirsig *et al.* (2016b); 7: Bichler *et al.* (2016). Numbers in white circles indicate sites in the eastern part of the eastern Alps where the LGM ice extent is constrained by ^{14}C and palynological data; 8: Borten-schlager (1984); 9: Starnberger *et al.* (2011); 10: Draxler, 1977; van Husen (1997); 11: Schmidt *et al.* (2002); 12: Schmidt *et al.* (2012). [Color figure can be viewed at wileyonlinelibrary.com]

on the LGM ice extent and the deglaciation history of the Gurktal and Lavantal Alps east of the Tauern Window. For these regions, Seguinot *et al.* (2018)'s model indicates an extensive LGM ice cover, whereas the mapped LGM ice margin (van Husen, 2011) implies that the glaciers only covered the Gurktal Alps while the Lavantal Alps farther east remained largely ice free during the LGM (Fig. 1). Our ^{10}Be age data show that the deglaciation of the Gurktal Alps (Nock Mountains) occurred between 16 and 14 ka, whereas ^{10}Be ages from the Lavantal Alps located farther east are either LGM in age or predate the LGM, indicating that these regions were not covered by an extensive LGM ice sheet. Together, the ^{10}Be data and DEM analysis provide important constraints on the position of the LGM ice margin and the deglaciation history of the easternmost Alps.

Geological setting and glacial history of the study area

Our study area comprises the Gurktal and Lavantal Alps, which are situated to the east of the Tauern Window (Figs. 1 and 2). The Gurktal Alps are confined along their western margin by the Katschberg normal fault and to the north and south by the Niedere Tauern and the Klagenfurt basin, respectively. To the east of the Katschberg normal fault, the Gurktal Alps include the Nock Mountains, which are characterised by subdued, hilly topography and a low relief, which is in marked difference to the higher topography and relief found in the adjacent Tauern Window and Niedere Tauern (e.g. Frisch *et al.*, 2000). The Lavantal Alps are located east of the Gurktal Alps and comprise the NNW–SSE-trending mountain ranges of the Saualpe and Koralpe (Fig. 2). Toward the east, the Koralpe is bordered by the Styrian Basin, which constitutes the western branch of the Pannonian Basin (Horváth *et al.*, 2006).

Geologically, both the Gurktal and Lavantal Alps belong to the Austroalpine unit and form part of the Adriatic microplate, which experienced a complex tectonic and metamorphic history from the Palaeozoic to the Cainozoic (Schuster *et al.*, 2013). From west to east, the Gurktal Alps mainly consists of rocks belonging to Ötztal Bundschuh and the Drauzug Gurktal nappe systems (Schuster *et al.*, 2013). In the regions of our sampling sites in the Nock Mountains, the crystalline basement consists of paragneisses, orthogneisses and garnet-micaschists. In contrast, the Saualpe and Koralpe (Lavantal Alps) comprise mainly Cretaceous high-pressure metamorphic rocks of the structurally lower Koralpe-Wölz nappe system (e.g. Thöni and Jagoutz 1992; Thöni and Miller, 1996; Schuster and Stüwe, 2008; Schuster *et al.*, 2013), in which Permo-Triassic low-pressure rocks have been preserved (Habler and Thöni, 2001). In the peak regions of the Saualpe and Koralpe, where our sampling sites are located, occur mainly paragneisses, mylonitic gneisses and micaschists.

During the LGM, major ice bodies filled the Drau and Mur valleys and also covered the Nock Mountains in the Gurktal Alps while only small cirque glaciers existed in the Lavantal Alps (Fig. 2) (van Husen, 2011). However, the age of moraines and other glacial features as well as the depositional age of erratic boulders and glacial till were mostly inferred indirectly

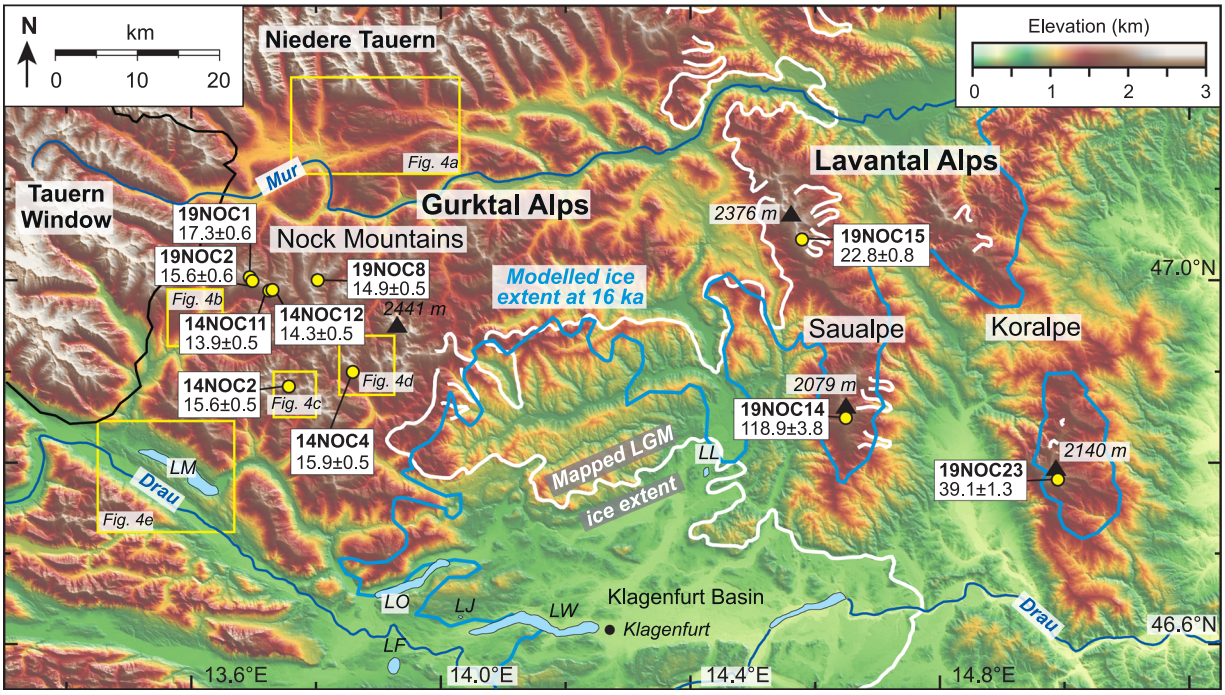

Figure 2. Study areas and sample locations with ^{10}Be ages (ka) in the Gurktal and Lavantal Alps, respectively. White line indicates LGM ice margin (Ehlers *et al.*, 2011; van Husen, 2011). Blue line marks ice margin at 16 ka in model from Seguinot *et al.* (2018). Yellow boxes outline areas shown in Fig. 4. Abbreviations are LF: Lake Faaker See; LJ: Lake Jeserzersee; LL: Lake Längsee; LM: Lake Millstätter See; LO: Lake Oissacher See; LW: Lake Wörthersee. [Color figure can be viewed at wileyonlinelibrary.com]

by correlation with sites, for which ^{10}Be, ^{14}C ages or palynological data were available, i.e. at the Traun valley mouth (Draxler, 1977, 1987; van Husen, 1977), in the Inn and Ötz valleys in Tyrol (Borten-schlager, 1984) or at the Julier Pass in Switzerland (Ivy-Ochs *et al.*, 1996, 2006a). As suggested for other regions in the eastern Alps, the LGM glacier extent and distribution in the Gurktal and Lavantal Alps are thought to be largely controlled by topography, because the eastern Alps are characterised by a more continental climate than the western Alps (Mayr and Heuberger, 1968; van Husen, 1989, 2011).

Melting of the LGM ice bodies began at *ca.* 20–19 ka in the foreland of the eastern Alps, as indicated by palynological, ^{14}C and OSL ages (van Husen, 1997; Reuther *et al.*, 2011; Starnberger *et al.*, 2011). Radiocarbon ages obtained from bulk sediment samples from the Carinthian Lake Jeserzersee located in the tongue area of the former Drau glacier suggest that the Klagenfurt Basin (Fig. 2) has been ice free since *ca.* 19–18 ka (Schmidt *et al.*, 2012). The inner-Alpine valleys were suggested to be ice free as early as ~19 ka (van Husen, 1997; Reitner, 2007) but little chronological control is available. For the Zillertal Alps (Tauern Window), Wirsig *et al.* (2016b) presented ^{10}Be exposure ages for bedrock samples taken at different altitudes. Exposure ages from the samples at the highest altitudes revealed that the lowering of ice surfaces in the high Alpine regions occurred between *ca.* 18.6 and 17.0 ka and hence somewhat delayed with respect to the downwasting of the glacier tongue (Wirsig *et al.*, 2016b). Samples from lower elevations yielded exposure ages of 16.4–14.8 ka, indicating that some ice patches persisted through the Gschnitz stadial (17–16 ka; Ivy-Ochs *et al.*, 2006b) until the Bølling-Allerød interstadial (Wirsig *et al.*, 2016b). During the following Egesen (Younger Dryas) stadial, glaciers advanced again (Ivy-Ochs *et al.*, 2006a; van Husen, 2011). In the Hohe Tauern Mountains, a Lateglacial glacier advance is documented by a sediment sequence, to which ^{10}Be and ^{14}C dating as well as pollen analyses were applied (Bichler *et al.*, 2016). The results showed that the sediment sequence consists of landslide deposits from the Bølling-Allerød interstadial overlain by glacial till and moraine material from the Egesen stadial, which, in turn, is overlain by landslide deposits from the Preboreal (Bichler *et al.*, 2016). In the Klagenfurt Basin, the cold period of the Younger Dryas is documented by an increase in the Alpine pine pollen content in a sediment record from Lake Längsee (Fig. 2) (Schmidt *et al.*, 2002).

Data and methods

^{10}Be exposure dating

Terrestrial cosmogenic nuclides including ^{10}Be are continuously produced in the uppermost metres below the Earth's surface by the interaction of cosmic rays (primary and secondary high-energy particles) with rocks (Dunai, 2010; Gosse and Phillips, 2001; Lal, 1991; Niedermann, 2002). The production rate of cosmogenic nuclides varies with altitude and latitude between a few atoms and several hundred atoms per gram per year and is determined from scaling-models for individual sampling sites (e.g. Balco *et al.*, 2008). Underground, the production rate decreases exponentially and becomes negligible (<5%) at a depth of >2 m (e.g. Niedermann, 2002). The exposure age of a bedrock surface can be computed from the measured ^{10}Be concentration and the local production rate, taking into account the thickness of the sample, its density, and the shielding of the sampling site from cosmic rays by the surrounding topography. Additional factors that can affect the exposure age are the erosion of the bedrock surface, which decreases the cosmogenic nuclide concentration, and potential shielding by snow, which lowers the local production rate. Both erosion and snow shielding result in apparent exposure ages that are younger than the true exposure age (e.g. Gosse and Phillips, 2001; Schildgen *et al.*, 2005).

Here, we apply ^{10}Be exposure dating to glacially polished quartz veins to constrain the timing of deglaciation. This approach assumes that at least the upper 2–3 m of bedrock have been eroded during the last glaciation, which removes the cosmogenic nuclide content inherited from prior periods of exposure (Balco, 2011; Dielforder and Hetzel, 2014; Dühnforth *et al.* 2010; Fabel *et al.*, 2004). Quartz veins can preserve extremely smooth glacially polished surfaces, which indicates that postglacial erosion is zero (e.g. Dielforder and Hetzel, 2014). Our sampling sites are located at about 2 km elevation in an Alpine environment with seasonal snow cover. To account for snow shielding, we estimated the length of the snow period (December–April) and average snow depths (70–100 cm) from nearby climate stations. The respective shielding factors were calculated following equation 3.76 in Gosse and Phillips (2001) and using a snow density of 0.3 g cm^{-3} (Jonas *et al.*, 2009) and an effective attenuation length of 160 g cm^{-2}.

Sampling strategy

We took samples in three different areas (Figs. 2 and 3; Table 1). The main set of samples was collected in the Gurktal Alps (Nock Mountains), which were covered by the LGM ice sheet, as indicated by mapping of glacial landforms (van Husen, 1997, 2011) and numerical modelling of the last glacial cycle in the European Alps (Seguinot *et al.*, 2018). Three additional samples were taken from the Saualpe and Koralpe, which are

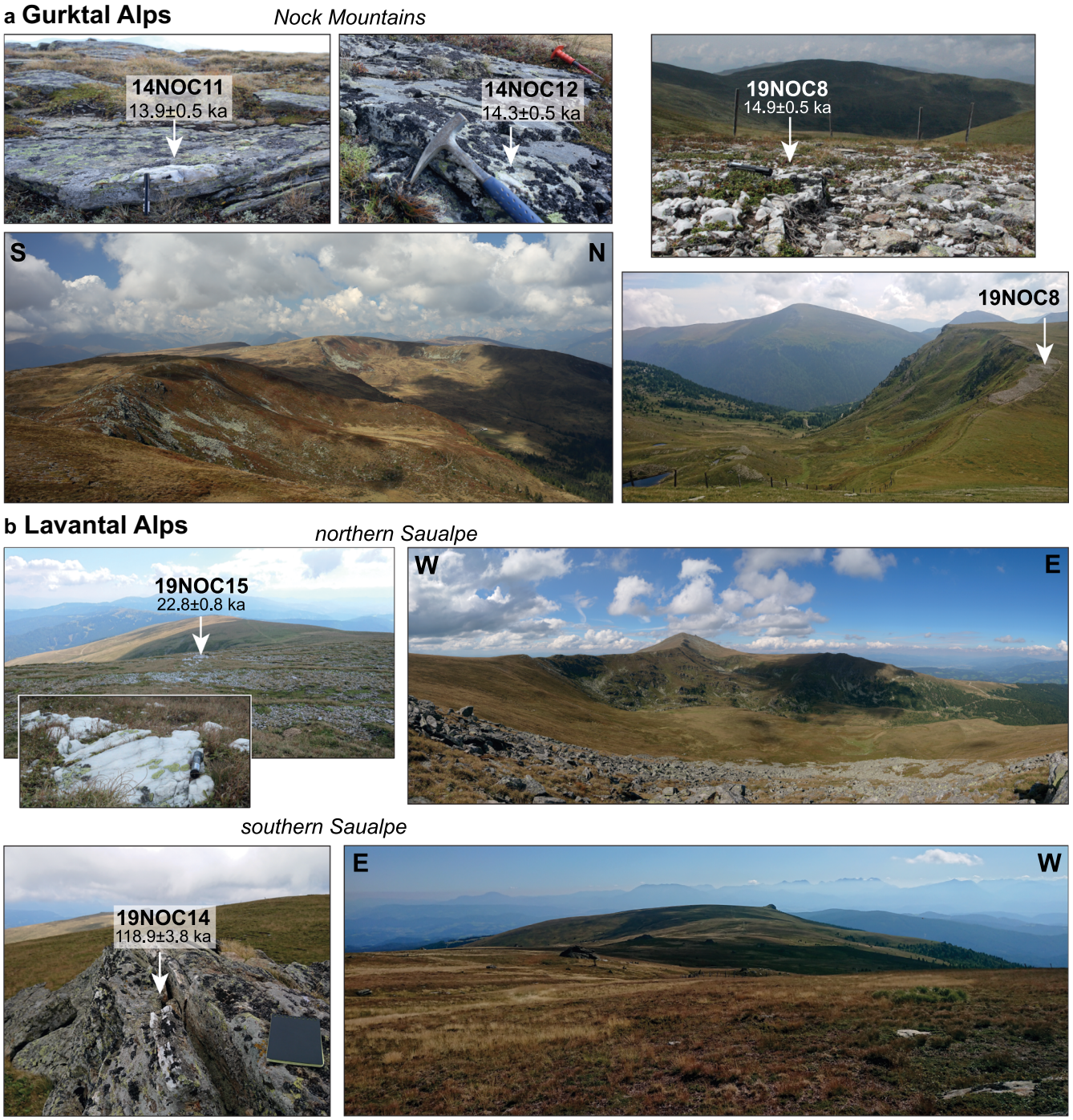

Figure 3. Field photographs of sampling sites (with obtained ^{10}Be exposure age) in (a) the Gurktal and (b) the Lavantal Alps. [Color figure can be viewed at wileyonlinelibrary.com]

Table 1. Sample locations, cosmogenic nuclide concentrations, shielding factors and calculated ^{10}Be exposure ages for the Gurktal and Lavantal Alps.

Sample number	Latitude (°N)	Longitude (°E)	Sample elevation (m)	Sample thickness (cm)	^{10}Be concentration[a] (10^4 at g^{-1})	Topographic shielding	^{10}Be exposure age[b] (ka)	Snow depth[c] (cm)	Snow shielding[d]	Snow-corrected ^{10}Be exposure age[b,e] (ka)
Gurktal Alps – Nock Mountains										
14NOC2	46.8836	13.7564	2050	3.5	32.08 ± 1.09	0.990	14.74 ± 0.50	80	0.942	15.58 ± 0.53 (1.07)
14NOC4	46.8998	13.8590	2058	3.5	33.09 ± 1.11	0.995	15.01 ± 0.51	80	0.942	15.89 ± 0.54 (1.09)
14NOC11	46.9883	13.7272	2138	3.5	30.26 ± 1.13	1.000	12.96 ± 0.49	100	0.929	13.87 ± 0.52 (0.97)
14NOC12	46.9894	13.7300	2185	3.5	32.46 ± 1.07	1.000	13.39 ± 0.44	100	0.929	14.34 ± 0.47 (0.97)
19NOC1	47.0033	13.6935	2150	5.0	37.97 ± 1.34	1.000	16.11 ± 0.57	100	0.929	17.29 ± 0.62 (1.20)
19NOC2	46.9991	13.6978	2095	5.0	32.84 ± 1.18	1.000	14.59 ± 0.53	100	0.929	15.64 ± 0.57 (1.09)
19NOC8	47.0001	13.8027	2154	3.0	33.06 ± 1.18	1.000	13.85 ± 0.49	100	0.929	14.86 ± 0.53 (1.03)
Lavantal Alps – Saualpe										
19NOC14	46.8492	14.6493	2048	4.5	250.8 ± 7.86	1.000	112.9 ± 3.64	70	0.949	118.9 ± 3.84 (8.18)
19NOC15	47.0447	14.5790	2189	3.5	54.18 ± 1.82	1.000	21.72 ± 0.74	70	0.949	22.82 ± 0.77 (1.56)
Lavantal Alps – Koralpe										
19NOC23	46.7814	14.9892	1982	3.5	79.60 ± 2.59	1.000	37.18 ± 1.22	70	0.949	39.11 ± 1.29 (2.66)

[a] ^{10}Be concentrations were measured at CologneAMS, Germany (Dewald *et al.*, 2013), and are normalised to the standards KN01-6-2 and KN01-5-3 with nominal ^{10}Be/^{9}Be ratios of 5.349×10^{-13} and 6.320×10^{-12}, respectively. We also analysed one aliquot of the quartz reference material CoQtz-N with a ^{10}Be concentration of $2.53 \pm 0.09 \times 10^6$ at g^{-1} (Binnie *et al.*, 2019), for which we obtained ^{10}Be concentrations of $2.57 \pm 0.09 \times 10^6$ at g^{-1}. The uncertainties of the ^{10}Be concentrations (1σ) include the analytical uncertainty and the error of the blank correction. The analytical uncertainty includes the error based on the counting statistics, the scatter of repeated measurements of the same sample, and the uncertainty of the standard normalisation.

[b] ^{10}Be exposure ages were calculated with the CRONUS-Earth ^{10}Be–^{26}Al online calculators (http://hess.ess.washington.edu/, version 3), using the time-dependent scaling model of Lifton *et al.* (2014), referred to as LSDn in the online calculator. All ages are corrected for topographic shielding and were calculated assuming a rock density of 2.65 g cm^{-3} and zero erosion. The errors after the age values are internal uncertainties, which include errors from the AMS counting statistics and the blank correction.

[c] The snow depths are average values from December to April derived from nearby climate stations for the time period 2010–2020.

[d] Snow shielding factors were calculated using a snow density of 0.3 g cm^{-3} (Jonas *et al.*, 2009) and an effective attenuation length of 160 g cm^{-2}.

[e] The errors given in parentheses are external errors that also include the uncertainty of the production rate and the uncertainty introduced by the scaling model.

part of the Lavantal Alps (Figs. 2 and 3; Table 1). For both Saualpe and Koralpe, mapping indicates that the sampling sites were located outside the extent of the LGM ice sheet (van Husen, 1997, 2011), whereas the ice-sheet models predict that they were covered by LGM ice until ~15 ka (Seguinot *et al.* 2018). All samples were collected at sites where a former cover by soil and vegetation can be considered unlikely.

Sampling preparation and ^{10}Be analysis

All samples were crushed, washed and sieved. Subsequently, the 250–500 µm grain-size fraction was split into a magnetic and non-magnetic fraction using a Frantz magnetic separator. The non-magnetic fraction was etched once in 6 M HCl at 80°C followed by four etching steps in diluted HF/HNO_3 in an ultrasonic bath at 80°C. For Be extraction, the purified quartz was dissolved in 40% HF after addition of 0.3 mg of Be carrier. After complete dissolution, all samples were converted into chloride form using 6 M HCl. Beryllium was separated by ion exchange column chemistry and precipitated as $Be(OH)_2$ at pH 8–9. Following the transformation to BeO at 1000°C, targets were prepared by mixing the BeO with Nb powder. All samples were analysed at the Centre for Accelerator Mass Spectrometry at the University of Cologne, Germany (CologneAMS; Dewald *et al.*, 2013).

Analysis of high-resolution DEMs for identification of glacial landforms and lineations

For the identification of glacial landforms and lineations in our study area, we used DEMs with a spatial resolution of 1 m. The DEMs were derived from Lidar (light detection and ranging) point cloud data and provided by the Austrian federal states Carinthia, Styria and Salzburg for download from the website https://www.data.gv.at (accessed March 2021). Among the geomorphological features that may be identified in high-resolution DEMs as indicators of former glaciations and ice flow directions are macroscale glacial striations, streamlined ridges such as drumlins, and roches moutonnées (e.g. Kelly *et al.*, 2004; Jansson and Glasser, 2005; Sookhan *et al.*, 2021).

Results

^{10}Be exposure ages

^{10}Be exposure ages were calculated with version 3 of the CRONUS-Earth ^{10}Be–^{26}Al online calculator (http://hess.ess.washington.edu; Balco *et al.*, 2008) using the time-dependent scaling model of Lifton *et al.* (2014), which is referred to as LSDn in the online calculator. For all calculations, we considered a rock density of 2.65 g cm^{-3}, zero erosion, and topographic shielding. All ^{10}Be exposure ages were calculated with and without snow shielding (Table 1). In the following, we report the snow-corrected exposure ages.

The ^{10}Be exposure ages from the Gurktal Alps range from 13.9 ± 0.5 ka to 17.3 ± 0.6 ka, whereas the three samples from the Lavantal Alps yielded ages of 22.8 ± 0.8 ka, 39.1 ± 1.3 ka and 118.9 ± 3.8 ka (Fig. 2, Table 1). The exposure ages from the Gurktal Alps are hence consistent with a deglaciation after the LGM, while the ages from the Lavantal Alps imply a longer exposure history. Below, we discuss the ^{10}Be exposure ages from the two regions in more detail.

Glacial landforms and lineations in the study area

The analysis of the high-resolution DEMs revealed that landforms indicative of former glaciation are abundant in the valleys and pass regions in the Gurktal Alps (Fig. 4). In the Mur valley, a swarm of drumlins occurs at the valley bottom (Fig. 4a). Macro-glacial striations can be identified along the valley bottom and the flanks of the adjacent mountains. Together, these features indicate former ice flow directions to the east (Fig. 4a). Glacial striations also occur along both flanks of the NNE–SSW-trending valley that marks the boundary between the Tauern Window and the Nock Mountains. Figure 4b shows the striations in the central section (called Katsch Valley) as an example. In the southern prolongation of the valley (called Lieser Valley), the glacial striations change their orientation and join the SE-trending lineations of the Drau Valley (Fig. 4e). A former south-eastward ice flow direction in the Drau valley is further indicated by elongated ridges at the valley bottom. In the Nock Mountains, macroscale glacial striations occur mainly in Alpine pass regions, including the areas around sampling sites 14NOC2 and 14NOC4 (Fig. 4c, d). At these passes, roches moutonnées indicate ice flow in south-western and south-eastern directions, respectively. For the Lavantal Alps, the DEM shows small glacial cirques (not shown in figure) but no signs of major glacial striations or glacially streamlined ridges.

Discussion

Our ^{10}Be exposure ages, which are the first data of this kind from the regions east of the Tauern Window, and our DEM analysis point to marked differences in the glacial history of the Gurktal and Lavantal Alps. Six of the seven ^{10}Be exposure ages from the Nock Mountains (Gurktal Alps) fall into the narrow range of *ca.* 16–14 ka (Fig. 2, Table 1), which indicates that erosion during the LGM and Lateglacial was sufficient to reset the ^{10}Be nuclide content. We therefore interpret the ^{10}Be ages from the Nock Mountains to reflect the timing of deglaciation when the glacially polished quartz veins became exposed due to melting of the ice cover. The slightly older age (17.3 ± 0.6 ka) of sample 19NOC1, which is located at an altitude of 2150 m and hence *ca.* 50 m higher than the nearby sample 19NOC2 (15.6 ± 0.6 ka) (Fig. 2), may reflect either an earlier thinning of the ice cover at this locality or a minor inherited ^{10}Be component due to insufficient erosion or brief exposure between the LGM and Oldest Dryas (Gschnitz stadial). Otherwise, our data do not show a correlation between exposure age and altitude of the sampling sites, which is in contrast to the findings by Wirsig *et al.* (2016b) in the Zillertal Alps. Compared with the Gurktal Alps, the three samples from the Lavantal Alps yielded higher and markedly different exposure ages (22.8 ± 0.8 ka, 39.1 ± 1.3 and 118.9 ± 3.8 ka), which imply a longer and probably more complex exposure history. In the following, we discuss the implications of our ^{10}Be exposure ages and DEM analysis for the glacial history of the Gurktal and Lavantal Alps.

Gurktal Alps

Our ^{10}Be exposure ages from the Nock Mountains (Gurktal Alps) show that this region was deglaciated between 16 and 14 ka (Fig. 5), i.e. at the transition from the Oldest Dryas to the Bølling-Allerød interstadial. In Carinthia, the Oldest Dryas to Bølling-Allerød transition was associated with a trend toward a warmer and wetter climate, as documented by the record from Lake Jeserzersee (Schmidt *et al.*, 2012). A comparison with the ^{10}Be age data from Wirsig *et al.* (2016b) further shows that the

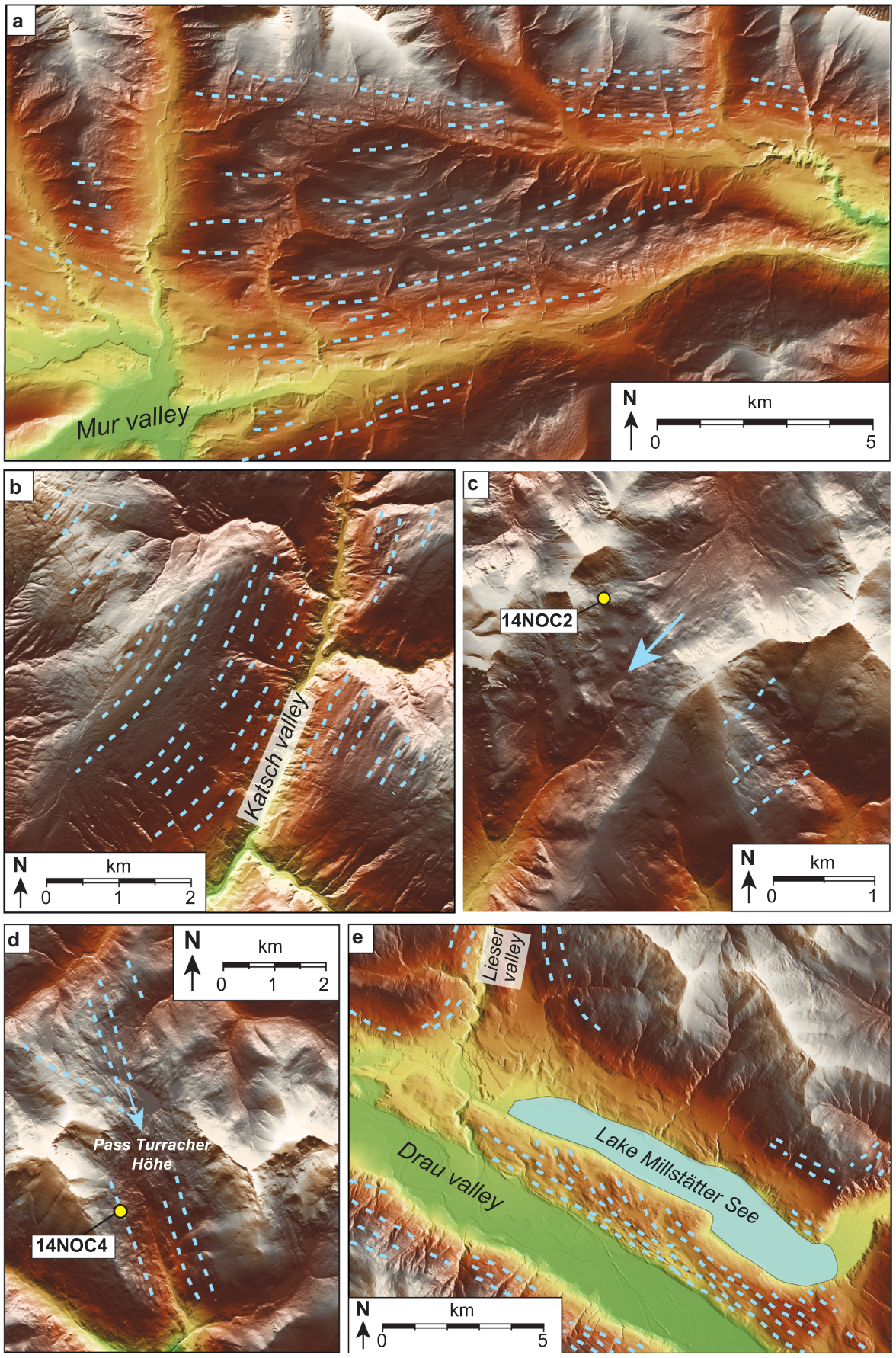

Figure 4. Topographic maps derived from high-resolution DEM showing examples of glacial lineations (traces indicated by dashed light blue lines) in the Gurktal Alps. (a) Mur Valley. (b) Katsch Valley. Area around sampling sites (c) 14NOC2 and (d) 14NOC4 in the Nock Mountains. (e) Drau Valley. [Color figure can be viewed at wileyonlinelibrary.com]

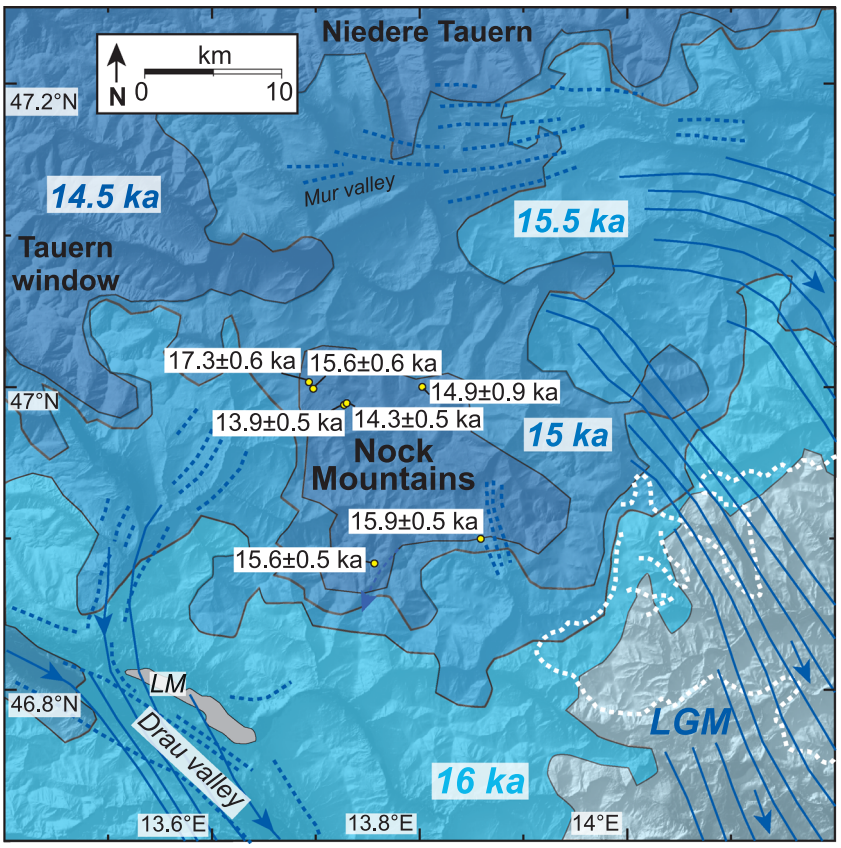

Figure 5. Map of the Gurktal Alps (Nock Mountains) showing the ^{10}Be data and macroscale glacial striations (this study, dashed blue lines) together with the mapped LGM ice extent (white dashed line; van Husen, 2011) and modelled LGM ice flow directions (solid blue lines) and Lateglacial ice margin positions (Seguinot *et al.*, 2018). LM: Lake Millstätter See. [Color figure can be viewed at wileyonlinelibrary.com]

deglaciation of the Nock Mountains occurred concurrently with the melting of the ice patches in the Zillertal Alps that had persisted through the Gschnitz (Oldest Dryas) stadial. Finally, our data are consistent with a spatially continuous ice coverage of the Nock Mountains from the LGM to *ca.* 15 ka (Fig. 5), as predicted by the ice-sheet model of Seguinot *et al.* (2018). Based on this comparison with Wirsig *et al.* (2016b) and Seguinot *et al.* (2018), our preferred interpretation is that the ice cover of the Nock Mountains persisted until deglaciation at *ca.* 15 ka, although this does not exclude the possibility that glaciers readvanced during the Gschnitz stadial following a brief retreat after the LGM. The ice flow directions indicated by the orientation of the glacially streamlined ridges and glacial lineations in the Gurktal Alps (Fig. 4) compare well with the modelled ice flow directions obtained by Seguinot *et al.* (2018). Both the glacial lineations in the DEM and modelled ice flow lines indicate that the glaciers followed and shaped the Drau, Mur and Katsch-Lieser valleys, whereas the ice flow across the Nock Mountains was more distributed with flow directions ranging from south-west to south-east (Figs. 4 and 5).

With respect to the LGM ice extent, we argue that the LGM ice covered a larger area in the Gurktal Alps than that mapped by van Husen (2011) for the following reasons. As mapped, the LGM ice margin would have been located only a few kilometres east of our sampling sites (Fig. 5), which would imply that the position of the ice margin along the eastern boundary of the Nock Mountains was almost stable from the LGM to *ca.* 16 ka. We consider this scenario unlikely because sediment records from the Klagenfurt Basin, i.e. the former Drau glacier tongue area (Fig. 2), and sites in the northern foreland of the eastern Alps (Fig. 1) indicate a fast retreat of glaciers over distances of up to 50–60 km from their LGM maximum position between 19 and 18 ka (van Husen, 1977; Schmidt *et al.*, 2002, 2012; Reuther *et al.*, 2011, Starnberger *et al.*, 2011). A comparison between the mapped LGM ice margin (van Husen, 2011) and the modelled ice margin at *ca.* 16 ka (Seguinot *et al.*, 2018) rather suggests that the ice margin mapped along the eastern boundary of the Nock Mountains and in an east–west direction toward the Saualpe represents the ice extent during the Gschnitz (Oldest Dryas; 17–16 ka) stadial (Fig. 2). A position of the LGM ice margin farther to the east of the Nock Mountains also appears more likely when considering that the glaciers must have reached a thickness sufficient to erode 2–3 m of bedrock, as indicated by the consistency of our ^{10}Be exposure ages.

Lavantal Alps

In contrast to the Gurktal Alps, the three ^{10}Be exposure ages obtained from samples in the Lavantal Alps are LGM in age or older (Table 1), i.e. these ages do not date the deglaciation after the LGM but record longer and probably more complex exposure histories. This finding argues against a thick, spatially continuous LGM ice cover of the Saualpe and Koralpe and a position of the LGM ice margin east of the Koralpe, which were predicted by the ice-sheet model (Fig. 1; Seguinot *et al.*, 2018). Rather, our data support Seguinot *et al.* (2018)'s conclusion that their ice-sheet model overestimates the ice extent in the easternmost Alps.

The youngest of the three exposure ages (22.8 ± 0.8 ka; 19NOC15) was obtained from the northern Saualpe. Our preferred interpretation of this age is that during the LGM, this site was at least partially covered by ice that was capable of eroding and reducing the ^{10}Be content that may have been accumulated before the LGM. Alternatively, if glacial erosion during the LGM was sufficient to eliminate all inherited ^{10}Be, the exposure age would indicate that the ice cover may have melted earlier than at sites along the northern eastern Alps (Fig. 1). In any case, the ^{10}Be exposure age of *ca.* 23 ka implies that the ice cover on the northern Saualpe may have been more extensive than mapped (Fig. 2), although presumably not

as extensive as modelled. In marked contrast to the northern Saualpe, the exposure age obtained from the southern Saualpe (118.9 ± 3.8 ka; 19NOC14) falls into the Eemian warm period (Marine Isotope Stage (MIS) 5e). We interpret this age to reflect the fact that the southern Saualpe was virtually ice free during the LGM. Considering that some erosion may have affected the sampling site would increase the age of sample 19NOC14 to 132 ka or 141 ka if we assume an erosion rate of 1 or 1.5 mm ka^{-1}, respectively (e.g. Dielforder and Hetzel, 2014). This would shift the age toward the end of the penultimate glaciation (MIS 6). A higher age than the obtained minimum ^{10}Be age seems even more likely when taking into account that the exposure history most likely comprised cold periods during which the shielding from snow cover may have been larger than today. As the sampling site still shows indications of ice moulding (Fig. 3b), our preferred interpretation therefore is that the quartz vein was exposed during deglaciation after the penultimate glacial period and that the age of sample 19NOC14 results from the combined effect of minor erosion and snow shielding. Our interpretation that the southern Saualpe was glaciated during MIS 6 (but not during the LGM) is consistent with observations indicating that the penultimate glaciation in the Alps was presumably more extensive than the last glaciation (Schlüchter, 2004; van Husen, 2011; Bickel *et al.*, 2015). Notably, similarly high exposure ages between 60–107 ka (^{10}Be) and 73–123 ka (^{21}Ne) were reported from erratic boulders deposited on a ridge in the Jura Mountains (Graf *et al.*, 2007). Considering erosion of the boulders that resulted in pre-Eemian exposure ages, Graf *et al.* (2007) argued that the boulders were deposited during the penultimate glacial period (MIS 6), which corresponds to the Rissian glaciation. Both findings, i.e. the position of the boulders above the LGM ice surface in the Jura Mountains and our ^{10}Be exposure age from the southern Saualpe, support the notion of an ice extent larger than at the LGM during the penultimate glacial period (Schlüchter, 2004; Preusser *et al.*, 2011; van Husen, 2011; Bickel *et al.*, 2015).

The exposure age of sample 19NOC23 (39.1 ± 1.3 ka) from the Koralpe falls into the Middle Würmian warm phase, which has been correlated with MIS 3 (Ivy-Ochs *et al.*, 2008). During this period, the foreland of the Alps was probably ice free (Schlüchter *et al.*, 1991). Although the extent of glacier advances during the previous Middle Würmian cold period (MIS 4) and the Early Würmian (MIS 5d) remains controversial (Ivy-Ochs *et al.*, 2008), we consider it unlikely that the age of 19NOC23 reflects the timing of ice retreat after these periods because the LGM (Late Würm) was presumably more extensive than the Early and Middle Würmian glaciations (Ivy-Ochs *et al.* 2008). Therefore, we interpret this site to have experienced a more complex exposure history, with, for example, a first exposure after MIS 6 and a subsequent partial ice coverage during the LGM, which was, however, not sufficient to fully reset the ^{10}Be content. A minor LGM ice cover may be supported by the maximum elevation of the Koralpe (2140 m), which is *ca.* 240 m lower than the northern Saualpe where the ice was presumably thicker and more extensive.

Implications for ice extent in the eastern Alps during the LGM and Lateglacial

Although the number of ^{10}Be exposure ages from the Gurktal and Lavantal Alps is still limited, our data already provide important constraints on the LGM and Lateglacial ice extent in these parts of the eastern Alps. For the Gurktal Alps, our data document deglaciation at *ca.* 16–14 ka and a position of the LGM ice margin considerably farther to the east than mapped (Fig. 2). Based on our data and a comparison with the ice-sheet model of Seguinot *et al.* (2018), we hypothesise that the ice margin mapped north of the former Drau glacier tongue area marks the ice extent at *ca.* 16 ka (Gschnitz stadial) (Fig. 2).

The two markedly different exposure ages from the Saualpe suggest that the LGM ice margin was located between its higher northern and lower southern parts rather than running northward along the western edge of the Saualpe (Fig. 2). Glaciers on the Koralpe may have been more extensive than mapped but whether they were isolated ice bodies or connected to the main LGM ice mass remains unresolved. To better constrain the position of the LGM and Lateglacial ice margins in this part of the eastern Alps, additional age data are required. With respect to ice-sheet models, our findings highlight that the model results provide a valuable framework for evaluating the age data. To improve the predictions about the evolution of ice bodies and glaciers in the Alps, the incorporation of hitherto neglected east–west gradients in temperature and precipitation would be highly desirable. Palaeoclimate reconstructions indicate that the northern Alps received less precipitation than the southern Alps during the LGM (Kuhlemann *et al.*, 2008; Monegato *et al.*, 2017), which resulted in a north–south gradient in temperature and/or precipitation that should also be considered in addition to an east–west gradient (Seguinot *et al.*, 2018; Visnjevic *et al.*, 2020). Together, more age data and refined ice-sheet models will enable an improved assignment of mapped glacial features to the different glacial periods.

Conclusions

Our results show that the deglaciation of the Gurktal Alps (Nock Mountains) occurred between 16 and 14 ka, which is in very good agreement with the timing indicated by the ice-sheet model of Seguinot *et al.* (2018) and suggests that the easternmost Alps have been longer and more extensively covered by LGM ice than indicated by mapping (Ehlers *et al.*, 2011). Such a greater ice cover is further supported by our analysis of high-resolution DEMs, which reveal glacially streamlined ridges and macroscale glacial striations consistent with modelled ice flow directions (Seguinot *et al.*, 2018). In contrast, the Lavantal Alps were ice free (southern Saualpe) or not massively glaciated (northern Saualpe, Koralpe) during the LGM. The contrasting exposure ages from the northern and southern Saualpe may indicate that the LGM ice margin was located between these two regions.

Our study underlines the importance of obtaining more age data for the largely undated glacial features and sedimentary sequences in the eastern Alps, from which LGM and Lateglacial ice extents have been reconstructed (Ehlers *et al.*, 2011, and articles therein). As the evolution of Alpine ice cover is linked to variations in precipitation and temperature, such tighter age constraints would also be essential for studies assessing the glacial–interglacial climate evolution of the European Alps (e.g. Kuhlemann *et al.*, 2008; Monegato *et al.*, 2017; Visnjevic *et al.*, 2020). A better knowledge of the LGM ice extent would also be crucial for models of postglacial isostatic rebound (e.g. Stocchi *et al.*, 2005; Norton and Hampel, 2010; Sternai *et al.*, 2020) because the position of the eastern LGM ice margin controls the ice volume and the crustal response to deglaciation in the easternmost Alps.

Acknowledgements. We thank the two anonymous reviewers for their constructive comments that improved the manuscript. We also thank Christiane Wenske and Anne Niehus for their help during

preparation of the samples for ^{10}Be exposure dating and the team of the CologneAMS for the timely analysis of all samples. Open Access funding enabled and organized by Projekt DEAL.

References

Balco G. 2011. Contributions and unrealized potential contributions of cosmogenic-nuclide exposure dating to glacier chronology, 1990-2010. *Quaternary Science Reviews* **30**: 3–27.

Balco G, Stone J, Lifton NA *et al*. 2008. A complete and easily accessible means of calculating surface exposure ages or erosion rates from ^{10}Be and ^{26}Al measurements. *Quaternary Geochronology* **3**: 174–195.

Batchelor CL, Margold M, Krapp M *et al*. 2019. The configuration of Northern Hemisphere ice sheets through the Quaternary. *Nature Communications* **10**: 3713.

Bichler MG, Reindl M, Reitner JM *et al*. 2016. Landslide deposits as stratigraphical markers for a sequence-based glacial stratigraphy: a case study of a Younger Dryas system in the Eastern Alps. *Boreas* **45**: 537–551.

Bickel L, Lüthgens C, Lomax J *et al*. 2015. The timing of the penultimate glaciation in the northern Alpine Foreland: new insights from luminescence dating. *Proceedings of the Geologists' Association* **126**: 536–550.

Binnie SA, Dewald A, Heinze S *et al*. 2019. Preliminary results of CoQtz-N: A quartz reference material for terrestrial in-situ cosmogenic ^{10}Be and ^{26}Al measurements. *Nuclear Instruments and Methods in Physics Research B* **456**: 203–212.

Borten-schlager S. 1984. Beiträge zur Vegetationsgeschichte Tirols I. Inneres Ötztal und unteres Inntal. *Berichte des naturwissenschaftlich-medizinischen Vereins Innsbruck* **71**: 19–56.

Braumann SM, Schaefer JM, Neuhuber SM *et al*. 2020. Holocene glacier change in the Silvretta Massif (Austrian Alps) constrained by new ^{10}Be chronology, historical records and modern observations. *Quaternary Science Reviews* **245**: 106493.

Clark PU, Dyke AS, Shakun JD *et al*. 2009. The Last Glacial Maximum. *Science* **325**: 710–714.

Darnault R, Rolland Y, Braucher R *et al*. 2012. Timing of the last deglaciation revealed by receding glaciers at the Alpine-scale: impact on mountain geomorphology. *Quaternary Science Reviews* **31**: 127–142.

Dewald A, Heinze S, Jolie J *et al*. 2013. CologneAMS, a dedicated center for accelerator mass spectrometry in Germany. *Nuclear Instruments and Methods in Physics Research Section B* **294**: 18–23.

Dielforder A, Hetzel R. 2014. The deglaciation history of the Simplon region (southern Swiss Alps) constrained by ^{10}Be exposure dating of ice-molded bedrock surfaces. *Quaternary Science Reviews* **84**: 26–38.

Draxler I. 1977. Pollenanalytische Untersuchungen von Mooren zur Spät- und postglazialen Vegetationsgeschichte im Einzugsgebiet der Traun. *Jahrbuch der Geologischen Bundesanstalt* **120**: 131–163.

Draxler I 1987. Zur Vegetationsgeschichte und Stratigraphie des Würmspätglazials des Traunglet-schergebietes. In *Das Gebiet des Traungletschers, O.Ö. Eine Typregion des Würm-GlazialsMitteilungen der Kommission für Quartärforschung der österreichischen Akademie der Wissenschaften*, van Husen D. (ed.). **7**: 19–35.

Dunai TJ. 2010. *Cosmogenic Nuclides. Principles, Concepts and Applications in the Earth Surface Science*. Cambridge University Press: Cambridge.

Dühnforth M, Anderson RS, Ward D *et al*. 2010. Bedrock fracture control of glacial erosion processes and rates. *Geology* **38**: 423–426.

Ehlers J, Gibbard PL, Hughes PD (eds). 2011. Quaternary glaciations - Extent and chronology. A closer look. *Developments in Quaternary Science* **15**: 15–28.

Fabel D, Harbor J, Dahms D *et al*. 2004. Spatial patterns of glacial erosion at a valley scale derived from terrestrial cosmogenic ^{10}Be and ^{26}Al concentrations in rock. *Annals of the Association of American Geographers* **94**: 241–255.

Federici PR, Granger DE, Pappalardo M *et al*. 2008. Exposure age dating and Equilibrium Line Altitude reconstruction of an Egesen moraine in the Maritime Alps, Italy. *Boreas* **37**: 245–253.

Frisch W, Székely B, Kuhlemann J *et al*. 2000. Geomorphological evolution of the Eastern Alps in response to Miocene tectonics. *Zeitschrift für Geomorphologie* **44**: 103–138.

Gosse JC, Phillips FM. 2001. Terrestrial in situ cosmogenic nuclides: theory and application. *Quaternary Science Reviews* **20**: 1475–1560.

Graf A, Strasky S, Ivy-Ochs S *et al*. 2007. First results of cosmogenic dated pre-Last Glaciation erratics from the Montoz area, Jura Mountains, Switzerland. *Quaternary International* **164–165**: 43–52.

Habler G, Thöni M. 2001. Preservation of Permo-Triassic low-pressure assemblages in the Cretaceous high-pressure metamorphic Saualpe crystalline basement (Eastern Alps, Austria). *Journal of Metamorphic Geology* **19**: 679–697.

Horváth FG, Bada P, Szafián G *et al*. 2006. Formation and deformation of the Pannonian Basin. In *Constraints from observational data, in European Lithosphere DynamicsGeological Society Memoir*, Gee DG, Stephenson RA (eds). **32**: 129–145.

Ivy-Ochs S, Schlüchter C, Kubik P *et al*. 1996. The exposure age of an Egesen moraine at Julier Pass, Switzerland, measured with the cosmogenic radionuclides ^{10}Be, ^{26}Al and ^{36}Cl. *Eclogae Geologicae Helvetiae* **89**: 1049–1063.

Ivy-Ochs S, Schäfer J, Kubik P *et al*. 2004. Timing of deglaciation on the northern Alpine foreland (Switzerland). *Eclogae geologicae Helvetiae* **97**: 47–55.

Ivy-Ochs S, Kerschner H, Reuther A *et al*. 2006a. The timing of glacier advances in the northern European Alps based on surface exposure dating with cosmogenic ^{10}Be, ^{26}Al, ^{36}Cl, and ^{21}Ne. In *Application of cosmogenic nuclides to the study of Earth surface processes: The practice and the potentialGeological Society of America Special Paper*, Siame LL, Bourlés, DL, Brown ET (eds). **415**: 43–60.

Ivy-Ochs I, Kerschner H, Kubik PW *et al*. 2006b. Glacier response in the European Alps to Heinrich Event 1 cooling: the Gschnitz stadial. *Journal of Quaternary Science* **21**(2): 115–130.

Ivy-Ochs S, Kerschner H, Reuther A *et al*. 2008. Chronology of the last glacial cycle in the European Alps. *Journal of Quaternary Science* **23**: 559–573.

Jansson KN, Glasser NF. 2005. Using Landsat 7 ETM + imagery and Digital Terrain Models for mapping glacial lineaments on former ice sheet beds. *International Journal of Remote Sensing* **26**: 3931–3941.

Jonas T, Marty C, Magnusson J. 2009. Estimating snow water equivalent from snow depth measurements in the Swiss Alps. *Journal of Hydrology* **378**(1): 161–167.

Kelly MA, Kubik PW, von Blanckenburg F *et al*. 2004. Surface exposure dating of the Great Aletsch Glacier Egesen moraine system, western Swiss Alps, using the cosmogenic nuclide ^{10}Be. *Journal of Quaternary Science* **19**: 431–441.

Kelly MA, Ivy-Ochs S, Kubik P *et al*. 2006. Chronology of deglaciation based on ^{10}Be dates of glacial erosional features in the Grimsel Pass region, central Swiss Alps. *Boreas* **35**: 634–643.

Kerschner H, Hertl A, Gross G *et al*. 2006. Surface exposure dating of moraines in the Kromer valley (Silvretta Mountains, Austria) – evidence for glacial response to the 8.2 ka event in the Eastern Alps? *The Holocene* **16**: 7–15.

Kuhlemann J, Rohling EJ, Krumrei I *et al*. 2008. Regional Synthesis of Mediterranean Atmospheric Circulation During the Last Glacial Maximum. *Science* **321**: 1338–1340.

Lal D. 1991. Cosmic ray labeling of erosion surfaces: in situ nuclide production rates and erosion models. *Earth and Planetary Science Letters* **104**: 424–439.

Lifton N, Sato T, Dunai TJ. 2014. Scaling in situ cosmogenic nuclide production rates using analytical approximations to atmospheric cosmic-ray fluxes. *Earth and Planetary Science Letters* **386**: 149–160.

Mayr F, Heuberger H 1968. Type areas of late glacial and post-glacial deposits in Tyrol, Eastern Alps. Proceedings VII. INQUA Congress 14, University of Colorado Studies, *Series in Earth Sciences* **7**. Glaciation of the Alps, Boulder/Colorado, 143–165.

Monegato G, Scardia G, Hajdas I *et al*. 2017. The Alpine LGM in the boreal ice-sheets game. *Scientific Reports* **7**: 2078.

Moran AP, Ivy-Ochs S, Schuh M *et al*. 2016a. Evidence of central Alpine glacier advances during the Younger Dryas-early Holocene transition period. *Boreas* **45**: 398–410.

Moran AP, Kerschner H, Ivy-Ochs S. 2016b. Redating the moraines in the Kromer Valley (Silvretta Mountains) – New

evidence for an early Holocene glacier advance. *The Holocene* **26**: 655–664.
Moran AP, Ivy-Ochs S, Christl M *et al*. 2017. Exposure dating of a pronounced glacier advance at the onset of the late-Holocene in the central Tyrolian Alps. *The Holocene* **27**: 1350–1358.
Niedermann S 2002. Cosmic-ray produced noble gases in terrestrial rocks. In *Noble Gases in Geochemistry and CosmochemistryReviews in Mineralogy and Geochemistry*, Porcelli D, Ballentine CJ, Wieler R (eds). **47**: 731–784.
Norton KP, Hampel A. 2010. Postglacial rebound promotes glacial readvances e a case study from the European Alps. *Terra Nova* **22**: 297–302.
Preusser F, Blei A, Graf HR *et al*. 2007. Luminescence dating of Würmian (Weichselian) proglacial sediments from Switzerland: methodological aspects and stratigraphical conclusions. *Boreas* **36**: 130–142.
Preusser F, Graf HR, Keller O *et al*. 2011. Quaternary glaciation history of northern Switzerland. *Quaternary Science Journal* **60**: 282–305.
Reitner J. 2007. Glacial dynamics at the beginning of Termination 1 in the Eastern Alps and their stratigraphic implications. *Quaternary International* **164/165**: 64–84.
Reuther AU, Fiebig M, Ivy-Ochs S *et al*. 2011. Deglaciation of a large piedmont lobe glacier in comparison with a small mountain glacier - new insight from surface exposure dating. Two studies from SE Germany. *Quaternary Science Journal* **60**: 248–269.
Schildgen TF, Phillips WM, Purves RS. 2005. Simulation of snow shielding corrections for cosmogenic nuclide surface exposure studies. *Geomorphology* **64**: 67–85.
Schlüchter C. 1991. Fazies und Chronologie des letzteiszeitlichen Eisaufbaues im Alpenvorland der Schweiz. In *Klimageschichtliche Probleme der letzten 130000 Jahre*, Frenzel B (ed.). G. Fischer: Stuttgart/New York; 401–407.
Schlüchter C. 2004. The Swiss glacial record—A schematic summary. In *Quaternary Glaciations: Extent and Chronology Part I: Europe*, Ehlers J, Gibbard PL (eds). Elsevier: London; 413–418.
Schmidt R, van den Bogaard C, Merkt J *et al*. 2002. A new Lateglacial chronostratigraphic tephra marker for the south-eastern Alps: the Neapolitan Yellow Tuff (NYT) in Längsee (Austria) in the context of a regional biostratigraphy and palaeoclimate. *Quaternary International* **88**: 45–56.
Schmidt R, Weckström K, Lauterbach S *et al*. 2012. North Atlantic climate impact on early late-glacial climate oscillations in the south-eastern Alps inferred from a multi-proxy lake sediment record. *Journal of Quaternary Science* **27**: 40–50.
Schuster R. 2003. Das eo-Alpine Ereignis in den Ostalpen: Plattentektonische Situation und interne Struktur des Ostalpinen Kristallin. *Geologische Bundesanstalt - Arbeitstagung* **2003**: 141–159.
Schuster R, Stüwe K. 2008. Permian metamorphic event in the Alps. *Geology* **36**: 603–606.
Schuster R, Kurz W, Krenn K *et al*. 2013. Introduction to the Geology of the Alps. *Berichte der Geologischen Bundesanstalt* **99**: 121–135.
Seguinot J, Ivy-Ochs S, Jouvet G *et al*. 2018. Modelling last glacial cycle ice dynamics in the Alps. *The Cryosphere* **12**: 3265–3285.
Sookhan S, Eyles N, Bukhari S *et al*. 2021. LiDAR-based quantitative assessment of drumlin to mega-scale glacial lineation continuums and flow of the paleo Seneca-Cayuga paleo-ice stream. *Quaternary Science Reviews* **263**: 107003.
Starnberger R, Rodnight H, Spötl C. 2011. Chronology of the Last Glacial Maximum in the Salzach Palaeoglacier Area (Eastern Alps). *Journal of Quaternary Science* **26**: 502–510.
Sternai P, Sue C, Husson L *et al*. 2020. Present-day uplift of the European Alps: Evaluating mechanisms and models of their relative contributions. *Earth-Science Reviews* **190**: 589–604.
Stocchi P, Spada G, Cianetti S. 2005. Isostatic rebound following the Alpine deglaciation: impact on the sea level variations and vertical movements in the Mediterranean region. *Geophysical Journal International* **162**: 137–147.
Thöni M, Jagoutz E. 1992. Some new aspects of dating eclogites in orogenetic belts: Sm-Nd, Rb-Sr, and Pb-Pb isotopic results from the Austroalpine Saualpe and Koralpe type-locality (Carinthia/Styria, southern Austria). *Geochimica et Cosmochimica Acta* **56**: 347–368.
Thöni M, Miller C. 1996. Garnet Sm-Nd data from the Saualpe and the Koralpe (Eastern Alps, Austria): chronological and P-T constraints on the thermal and tectonic history. *Journal of Metamorphic Geology* **14**: 453–466.
van Husen D. 1977. Zur Fazies und Stratigraphie der jungpleistozänen Ablagerungen im Trauntal. *Jahrbuch der Geologischen Bundesanstalt* **120**: 1–130.
van Husen D. 1989. The last interglacial glacial cycle in the Eastern Alps. *Quaternary International* **3/4**: 115–121.
van Husen D. 1997. LGM and Late-glacial fluctuations in the Eastern Alps. *Quaternary International* **38/39**: 109–118.
van Husen D. 2004. Quaternary glaciations in Austria. In *Quaternary Glaciations: Extent and Chronology Part I: Europe*, Ehlers J, Gibbard PL (eds). Elsevier: London; 1–13.
van Husen D 2011. Quaternary Glaciations in Austria. In *Quaternary Glaciations – Extent and Chronology: A Closer Look*, Ehlers J, Gibbard PL, Hughes PD (eds). **15**: 15–28.
Visnjevic V, Herman F, Prasicek G. 2020. Climatic patterns over the European Alps during the LGM derived from inversion of the paleo-ice extent. *Earth and Planetary Science Letters* **538**: 116185.
Wirsig C, Zasadni J, Ivy-Ochs S *et al*. 2016a. A deglaciation model of the Oberhasli, Switzerland. *Journal of Quaternary Science* **31**: 46–59.
Wirsig C, Zasadni J, Christl M *et al*. 2016b. Dating the onset of LGM ice surface lowering in the High Alps. *Quaternary Science Reviews* **143**: 37–50.